Model-Based Conifer Canopy Surface Reconstruction from Photographic Imagery: Overcoming the Occlusion, Foreshortening, and Edge Effects

Yongwei Sheng, Peng Gong, and Gregory S. Biging

Abstract

Canopy surface data are desirable in forestry, but they are difficult to collect in the field. Existing surface reconstruction techniques cannot adequately extract canopy surfaces, especially for conifer stands. This paper develops an integrated model-based approach to reconstruct canopy surface for conifer stands analytically from the crown level. To deal with dense stands, critical problems are addressed in the process of model-based surface reconstruction. These include the occlusion problem in disparity (parallax) prediction from tree models, the edge effect of tree models on the disparity map, and the foreshortening effect in image matching. The model-based approach was applied to recover the canopy surface of a dense redwood stand using images scanned from 1:2,400-scale aerial photographs. Compared with field measurements, crown radius and tree height derived from the reconstructed canopy surface model have an overall accuracy of 92 percent and 94 percent, respectively. The results demonstrate the approach's ability to reconstruct complicated stands.

Introduction

The form of a tree crown is an indicator to species competition in a stand. A canopy surface describes the geometric shape of the canopy and indicates photosynthetic ability and biomass. Information on crown form and canopy structure is an important determinant of wildlife habitat preferences for many species of birds and mammals (Biging and Gill, 1997). Data on canopy surface are needed to produce orthophotos and derive distortion-free forest parameters.

Although canopy surfaces are important in forestry and ecological studies, they are rarely measured in forest inventory due to the difficulty in measuring 3D canopy surfaces from the ground and the lack of success in existing surface reconstruction techniques. Quackenbush *et al.* (1999) used Desktop Mapping System (DMS®) to derive tree canopy surfaces from 1-m resolution aerial photographs, and pointed out that the unsuccessful canopy surface reconstruction may be due to the constraint of the package used. Our experiments with a number of other commercial softcopy photogrammetry packages led to similar failures[1]. Current commercial packages are not designed to extract canopy surfaces with high variability in the vertical direction.

Sheng *et al.* (2001) introduced a model-based photogrammetric approach to tree crown surface reconstruction. They expressed the crown morphology of a tree using 3D geometric models and modeled it as a generalized 3D hemi-ellipsoid. They manually established the optimal tree model from aerial photos, and used the initial crown surface derived from the tree model to guide image matching in crown surface reconstruction. The potential of this model-based approach was demonstrated using a single tree. When reconstructing the canopy surface of a dense stand of multiple trees, we need to establish optimal tree models in a more efficient manner and consider problems such as occlusion. This paper extends the capability of the model-based approach from recovering the crown surface of a single tree to reconstructing the canopy surface of a tree stand, and further develops the model-based method to canopy surface reconstruction for complicated tree stands. The improved method addresses the problems of occlusion, foreshortening, and tree edge effects, and was applied to reconstructing the canopy surface for a dense redwood stand. The reconstructed canopy surface was validated using dimensional crown measurements from the field and crown profile pictures taken from various directions on the ground.

Study Site and Data Preparation

The study area is located on the campus of the University of California at Berkeley (122.38°W, 37.62°N). The test was carried out in an uneven-aged redwood-dominant stand of nearly 100 percent canopy closure using 1:2,400-scale aerial photographs. The difference in ground elevation at this site is less than 10 m. The study area is about 170 m long and 120 m wide containing several oak (*Quercus kelloggii*) and approximately 60 redwood (*Sequoia sempervirens*) trees, the latter of which are up to 45 m in height.

Bi-ocular images may be insufficient for conifer canopy surface reconstruction due to the occlusions caused by sharp

Center for Assessment and Monitoring of Forest and Environmental Resources (CAMFER), 145 Mulford Hall, University of California, Berkeley, CA 94720-3114 (gong@nature.berkeley.edu; biging@nature.berkeley.edu).

Y. Sheng is presently with the Department of Geography, 1255 Bunche Hall, University of California, Los Angeles (UCLA), Los Angeles, CA 90095-1524 (ysheng@geog.ucla.edu).

[1]Sheng, Y. "Tree height derivation from stereopairs–A test," unpublished report, Department of Environmental Science, Policy, and Management, University of California at Berkeley, May 1997, 12 p.

Photogrammetric Engineering & Remote Sensing
Vol. 69, No. 3, March 2003, pp. 249–258.

0099-1112/03/6903–249$3.00/0

crown morphology. We used tri-ocular high-resolution aerial images: one nadir view and two off-nadir views, so that most parts of a crown surface are visible on at least two images.

1:2,400-scale vertical aerial photographs were taken on 23 May 1994 with a camera whose focal length was 152.8 mm. Most of the stand is visible on three overlapping photographs, labeled as #2, #1 (the nadir view), and #0, respectively, from left to right. The adjacent photos have about 60 percent overlap, and the pair of #2 and #0 has about 20 percent overlap. These photographs were scanned at 250 DPI (dots per inch), making the pixel resolution approximately 24 cm on the ground. The camera station locations and camera attitudes of the three photos were solved through photogrammetric orientation procedures. Three overlapping photos form three stereo pairs. The original photos were resampled according to the epipolar geometry to generate three stereo pairs covering the study area: the 2-1 pair, the 2-0 pair, and the 1-0 pair.

Field measurements were collected in October 1999. Though there is a 5-year time lag between the field measurements and aerial photographs, most trees in the stand are mature and are not expected to grow much (e.g., several meters) during this period. We first delineated individual trees on the nadir view image (i.e., #1) by visual interpretation, and made a sampling map (Figure 1) to guide our fieldwork. Tree height and crown radii from four perpendicular directions (i.e., south, west, north, and east) were measured for 38 trees using clinometers and tapes. Some ground pictures were taken from various directions to record crown profiles. These field measurements and pictures were used to validate the reconstructed canopy surface.

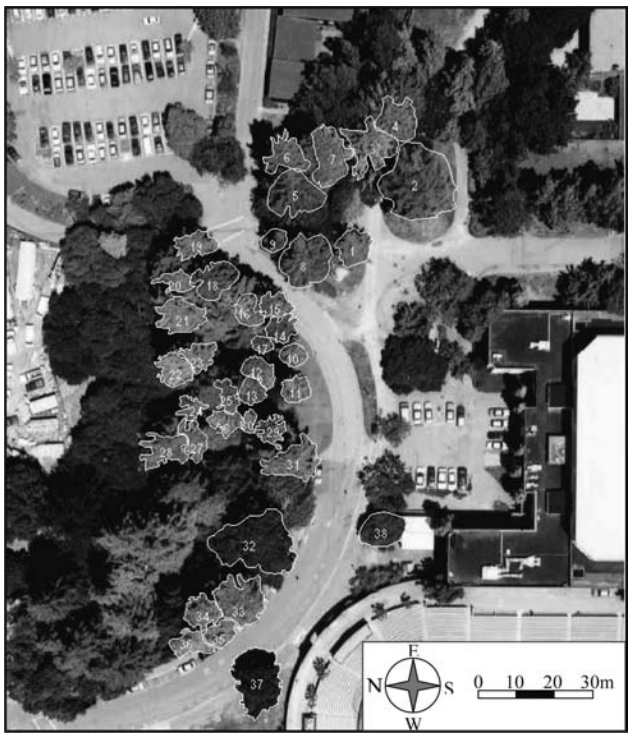

Figure 1. The sampling map. It was generated by visually delineating individual trees on the nadir view image. Thirty-eight trees were measured in the field using this map as a guide.

Methods

Geometric Modeling of Trees and Optimal Tree Model Development

Geometric models were used in tree modeling for their simplicity in parameterization. On the basis of Horn's 2D (Horn, 1971) and Pollock's 3D (Pollock, 1996) geometric crown models, Sheng *et al.* (2001) extended the 3D crown model to a 3D tree model for the purpose of applying the tree model to crown surface reconstruction. This tree model uses a generalized hemi-ellipsoid crown model, and is described by three location parameters: ground coordinates of the treetop (X_{top}, Y_{top}, Z_{top}); and three parameters on crown dimensions: crown depth (ch), crown radius (cr), and an adjusting coefficient for crown curvature (cc). Once these parameters are known, the tree model is fixed and the ground coordinates (X, Y, Z) of any point on the crown surface can be modeled by

$$\frac{(Z + ch - Z_{top})^{cc}}{ch^{cc}} + \frac{((X - X_{top})^2 + (Y - Y_{top})^2)^{cc/2}}{cr^{cc}} = 1 \quad (1)$$

where $Z_{top} - ch \le Z \le Z_{top}$.

To make the model-based approach practical in canopy surface reconstruction of forest stands, optimal tree models need to be established efficiently from the aerial images for individual trees. Sheng (2000) discussed both the automatic and semiautomatic scenarios for tree model development. The automatic scheme is computationally intensive, and it often fails for complicated stands. As an alternative, a model-based 3D tree interpreter was built with a semiautomatic approach to optimal tree model development (Gong *et al.*, 2002). The conjugated treetops of a tree are sampled interactively on the 2-0 photo pair to obtain the ground coordinates (X_{top}, Y_{top}, Z_{top}) of the treetop, and the dimensional parameters of the crown are determined semiautomatically on informative images. The 3D tree interpreter is able to establish reliable tree models for complicated tree stands efficiently.

In addition to the optimal tree models, a background DEM (digital elevation model) is another product of the 3D tree interpreter. During tree interpretation, the elevations of some visible tree bases and ground points were sampled on the photos, and a DEM was interpolated from these sampled points.

Occlusion Removal in Disparity Prediction

Disparity, also known as parallax, is the coordinate difference of a point imaged on two photos taken from different angles. The disparity between the two conjugated pixels in the photos can be used to reconstruct the elevation value of the point in object space. Disparity is usually derived using image matching. Because the background DEM and the optimal tree models were produced at the tree interpretation stage, we can use them to predict the initial disparity map, and then use the initial disparity map to guide subsequent image matching. The ground coordinates of each point on a tree crown surface can be calculated from its tree model using Equation 1. The disparity of a point on a crown surface or on the ground surface can be predicted using the collinearity equations in photogrammetry. However, disparity prediction from tree models can be problematic for dense stands, and occlusion has to be taken into account. Z-buffer techniques, which are one of the general techniques in computer graphics for hidden surface removal (Pokorny and Gerald, 1989), were used to address this problem. They are based on the fact that foreground objects occlude background objects, and they use a depth buffer (Z-buffer) to record depth information, which is critical to determine which object occludes others.

The Z-buffer algorithm for occlusion removal in disparity prediction is shown in Figure 2. The buffer here records the distance between the camera station and surface point being imaged.

```
/* Inputs:
   Trees                                  /* Tree models
   S=(Xs, Ys, Zs)                         /* Camera station
   A=(φ, ω, κ)                            /* Camera attitude
   DEM                                    /* The background DEM
/* Initializing:
   Disparity=Blank;                       /* The disparity map
   ZBuffer=a large number;                /* The depth buffer
/*Beginning
   /* Computing disparities from the background DEM
   FOR each cell C in DEM
      {
        calculate distance, the distance between C and S;
        project cell C to cell (i, j) in the disparity map;
        IF distance<ZBuffer(i, j)
           {
             ZBuffer(i, j)=distance;
             calculate disparity d of cell C;
             Disparity(i, j)=d;
           }
      {
   /* Computing disparities from tree models
   FOR tree k in Trees
      {
        FOR a point P on the surface of Trees(k)
          {
            calculate the ground coordinates (Xp, Yp, Zp) of P;
            calculate distance, the distance between P and S;
            project point P to cell (i, j) in the disparity map;
            IF distance<ZBuffer(i, j)
                {
                  ZBuffer(i, j)=distance;
                  calculate disparity d of point P;
                  Disparity(i, j)=d;
                }
          }
      }
/* End
/* Outputs:
   Output Disparity as the predicted disparity map.
/* Finish.
```

Figure 2. The Z-buffer algorithm for occlusion removal in disparity prediction.

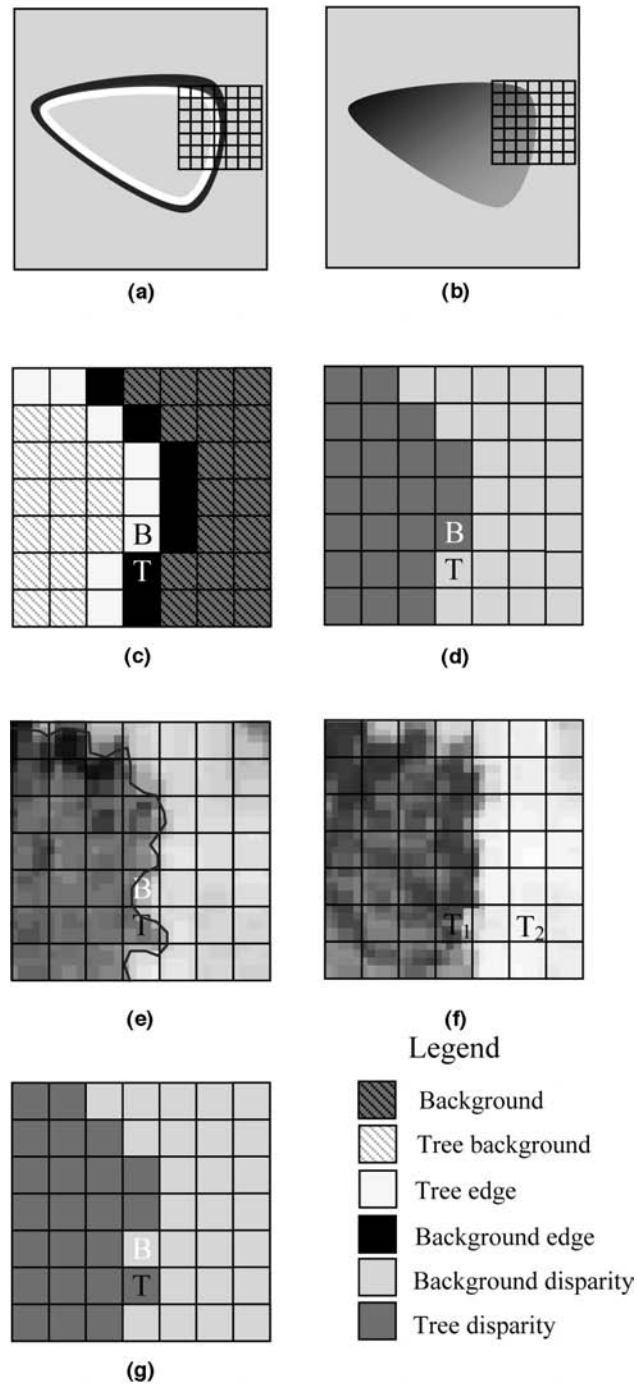

Figure 3. An illustration of the process of tree-edge effect reduction. (a) Tree edge and background edge of a tree. (b) Predicted disparity map of the tree. (c) and (d) A zoom-in window of (a) and (b). (e) and (f) Left and right aerial images of the zoom-in window. (g) Disparity map after tree-edge effect reduction.

Tree-Edge Effect Reduction in Disparity Map

The predicted disparity map from tree models has a distinctive contrast at the perimeter of tree canopies. However, the edges of tree canopies are usually "fuzzy" due to extended branches; thus, the sharp tree-edge effect should be reduced in the predicted disparity map.

Figure 3 illustrates the process of edge-effect reduction. We first generated an edge map from the tree models. The map contains both tree edges and background edges, and the background can either be the ground or tree canopies. A tree edge is a 1-cell-wide edge consisting of the tree cells next to background cells, while a background edge is the one containing the background cells next to tree cells. The edge map in Figure 3a shows the tree edge in white and the background edge in black around a tree. When the optimal tree model is not perfect, some cells on the tree edge could in fact be background-edge cells, and some cells on the background edge could be tree-edge cells. Figure 3b shows a typical disparity map predicted from a tree model. Figures 3c and 3d zoom into the portion within the grid in Figures 3a and 3b so that individual cells are visible. If a cell on the tree edge is actually from the background, then we need to modify the disparity map by replacing the disparity of this cell with that of a nearby background cell, and vice versa. Comparing the edge map with the left image (Figure 3e), we can see that the tree-edge cell at (row 5, column 4) marked by **B** should be a background cell, and that the background-edge cell at (6, 4) marked by **T** should be a tree cell.

We use the left and right aerial images (Figures 3e and 3f) to

assist decision making about the replacement. We determine whether an edge cell needs to be switched using the correlation coefficients between the templates around this cell on the left and right images. Suppose the template in the left image around this cell is $\mathbf{M_1}$. When the disparity of this cell is known, its position in the right image and the template around this position can be determined. If the disparity is taken from a tree cell, let the template in the right image be $\mathbf{M_{2t}}$. Similarly, if the disparity is from a nearby background cell, let the template be $\mathbf{M_{2b}}$. Let the correlation coefficient be $\mathbf{R_t}$ between $\mathbf{M_1}$ and $\mathbf{M_{2t}}$, and be $\mathbf{R_b}$ between $\mathbf{M_1}$ and $\mathbf{M_{2b}}$. If $\mathbf{R_b} > \mathbf{R_t}$, then this cell should be switched to the background cell and take the background disparity; otherwise, the tree disparity should be kept. As illustrated in Figures 3e and 3f, two positions $\mathbf{T_1}$ and $\mathbf{T_2}$ in the right image of cell **T** are determined using the tree disparity and the background disparity, respectively. The correlation between the templates around **T** and $\mathbf{T_1}$ is higher than that between **T** and $\mathbf{T_2}$; therefore, cell **T** takes the tree disparity. Similarly, cell **B** takes the background disparity. The resulting disparity map is shown in Figure 3g. Using this procedure, we can mitigate the edge effect introduced by imperfect tree models. Figure 4 shows the adjusted disparity map, in which the tree edges appear less regular and the occlusion problem was properly addressed. For the portion of trees extending beyond the study area, the edge effect was not adjusted because no background DEM was available.

Foreshortening Effect Mitigation in Stereo Matching

An image matching (or correspondence finding) algorithm is the core of photogrammetric surface reconstruction. Correlation-based image matching approaches are widely used. Suppose the range of disparity between the left and right images is $[-D, D]$ (unit: pixels). As illustrated in Figure 5, the correlation calculation produces a similarity space, a 3D correlation cube of $2D + 1$ depth containing the correlation coefficients (Chen and Medioni, 1999). The voxel (volume element) at location (i, j, d) in the cube records the correlation coefficient between a template around pixel (i, j) in the left image and a template of the same size around the pixel $(i, j + d)$ in the right image. The correlation coefficient however is vulnerable to the foreshortening effect.

A surface patch will appear foreshortened unless it is viewed from its normal direction (Klaus and Horn, 1986). This is the so-called "foreshortening effect." The resulting problem of the foreshortening effect in stereo matching is that the surface patches in the two templates, with which an image matching algorithm intends to match, are not of the same size. The foreshortening effect in canopy surface reconstruction is very serious due to the steep tree crown surfaces, and is one of the major causes of reconstruction failures.

We use the matching-on-orthoimage approach to mitigate the foreshortening effect (Norvelle, 1992; Schenk and Toth, 1992; Norvelle, 1996). Figure 6 compares how the image templates are matched for a point on a crown surface before and after the foreshortening effect is addressed. Figures 6a and 6b show the portion of the original left and right images containing a redwood tree (i.e., Tree #1). Due to the foreshortening effect, the right side of the tree crown in the right image is almost three times as long as that in the left image. The two templates (outlined by the white boxes) do not match for the same surface patch; thus, the correlation measure between them is not reliable. This effect is mitigated by matching on orthoimages. Figures 6c and 6d show the left and right orthoimages of the same area in Figures 6a and 6b. The two templates are virtually of the same patch, and the foreshortening effect disturbs the correlation measure between the templates to a much less

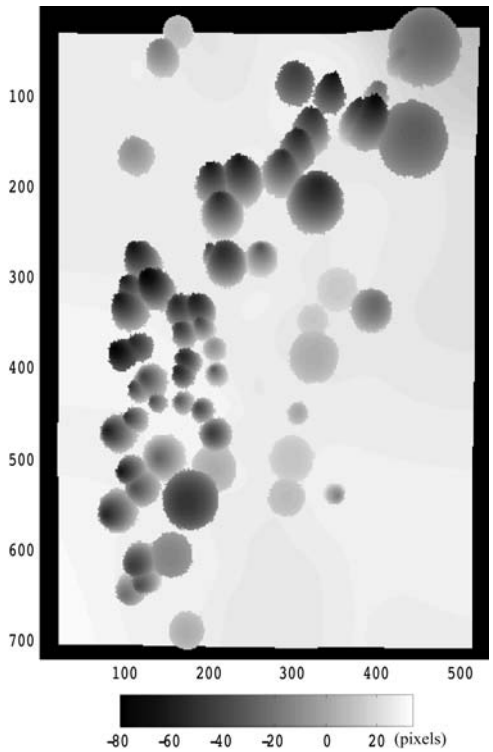

Figure 4. The disparity map after tree-edge effect reduction. This map was predicted from the background DEM and the optimal tree models. The occlusion problem was properly addressed, and the tree-edge effect was reduced.

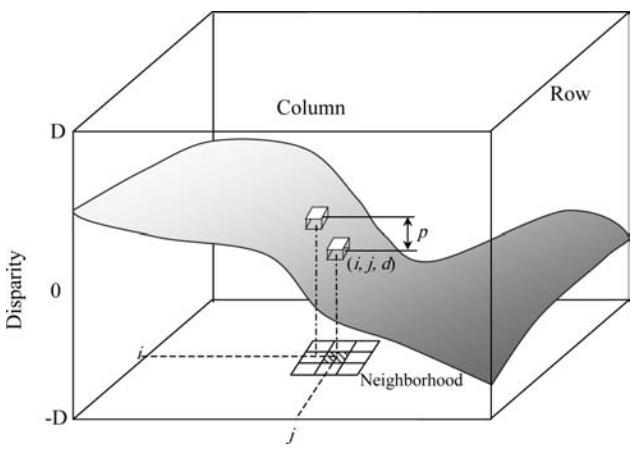

Figure 5. The 3D correlation cube. The correlation computation in image matching generates a 3D correlation cube. The voxel at location (i, j, d) in the cube records the correlation coefficient between a template around pixel (i, j) in the left image and a template of the same size around the pixel $(i, j + d)$ in the right image. The dynamic programming image-matching algorithm determines the disparity map by searching in the 3D correlation cube for the maximum p-ordered smooth surface. The parameter D specifies the disparity range and determines the depth of the correlation cube, while p controls the smoothness of the surface to be found.

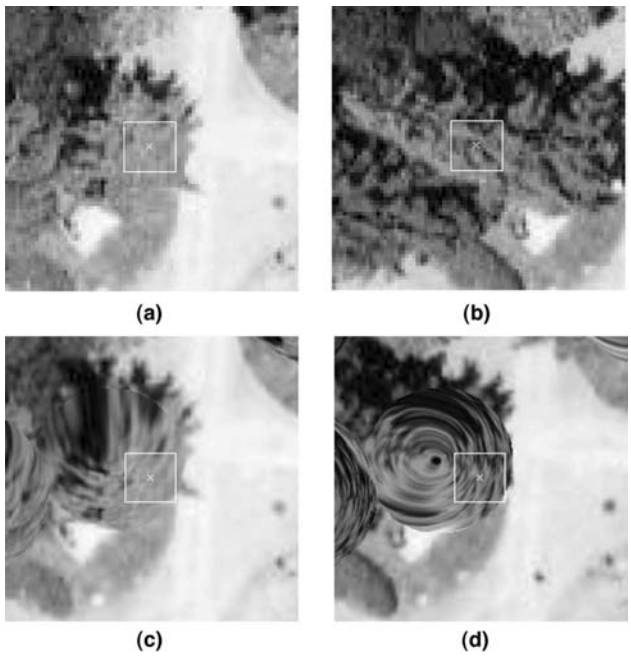

Figure 6. Matching windows for reduction of the foreshortening effect. (a) Left perspective image; (b) Right perspective image. (c) Left orthoimage. (d) Right orthoimage. Due to foreshortening, the right side of the tree crown in the right image in (b) is almost three times as long as that in the left image in (a). The two templates (outlined by the white boxes) do not match for the same surface patch; thus, the correlation measure between them is not reliable. When matching on orthoimages in (c) and (d), the two templates are virtually of the same patch, and the foreshortening disturbs the template matching at a largely reduced level.

extent. In such a way, we incorporate the reduction of the foreshortening effect in the correlation cube generation.

An image-matching algorithm is needed to find correspondence based on the correlation cube. We adopted a dynamic programming algorithm for the image matching scheme because it simultaneously uses many important constraints such as those of epipolar planes, photometric compatibility, uniqueness, disparity continuity, and disparity limit (Marr, 1982; Sun, 1999).

The dynamic programming algorithm is a global matching method, and determines the disparity map by searching in the 3D correlation cube (Figure 5) for the maximum smooth surface characterized by surface order p (Sun, 2002). That is, the neighbors of a voxel on the p-ordered surface are within p voxels in the vertical dimension, and the sum of the correlation measures of all voxels on the surface reaches the maximum. As illustrated in Figure 5, D specifies the disparity range and determines the depth of the correlation cube, while p controls the smoothness of the surface to be found. Dynamic programming using smaller p searches for a smoother disparity surface in the cube, and generates a smoother surface model for the canopy.

The model-predicted disparities serve as a guide to correspondence finding. They can be considered as the general trend, and only the detailed local variations need to be extracted. Therefore the search for the p-order surface can be usually limited to a small disparity range $[-D, D]$ around the predicted disparities. When the range is large, the dynamic programming algorithm is implemented under the pyramidal image-matching scheme for both efficiency and reliability.

Matching Control and Iteration

The disparity limit D and the surface order p play an important role in image matching by dynamic programming. When the dynamic programming algorithm searches for the disparity surface in the correlation cube, surface order p can be set to various values between 0 and D. The selection of D and p depends on the confidence in the optimal tree models. If these tree models perfectly describe the crown surfaces, then both D and p are set to zero, meaning no adjustment is needed. If the tree models are only a rough approximation of the true crown surfaces, then both D and p need to be increased, and this will introduce more variations into the reconstructed canopy surface.

The geometric form of individual trees in a stand may vary. Some trees may be well described by their tree models, while others may not. Small D and p are desirable for regular-shaped trees, but may generate a regular surface for irregular-shaped trees. This makes it difficult to choose universal values of D and p. We can mitigate this problem by iterating the matching process. The approach discussed here can be implemented as an iterative procedure. Even when the knowledge about tree shape is poor, the initial values for D and p can be set to small values. The output from the first round model-based matching can be used as the initial condition in the next round model-based matching, enabling gradual adjustments to the derived surface. This procedure could be repeated until the results are satisfactory. With such an iterative approach, regular-shaped trees are more likely to find their matches in earlier rounds, while irregular-shaped trees may find theirs in later rounds.

Sophisticated Model-Based Canopy Surface Reconstruction Scheme

With the problems of occlusion, foreshortening, and edge effects considered, a sophisticated model-based canopy surface reconstruction scheme is illustrated in Figure 7. After the optimal tree models and the background DEM have been developed in 3D tree interpretation, we use them to predict an initial disparity map and to compose the initial digital surface model (DSM). The disparity map is then processed for tree-edge effect reduction. Orthoimages are produced using the DSM to reduce the foreshortening effect in the correlation cube. The value of each cell in the generated disparity map may be adjusted by a number of pixels in the disparity range $[-D, D]$. For each adjustment within the range, the corresponding locations in the left and right orthoimages can be calculated, and a correlation measure is computed using the templates from orthoimages at the locations found. In such a way, the correlation cube is generated using orthoimages rather than the perspective images, thus is less vulnerable to the foreshortening effect. A new DSM is reconstructed by searching for the maximum disparity surface in the correlation cube using the dynamic programming technique. If the DSM is satisfactory, then it is the final canopy model; otherwise, the process is repeated using the new DSM as the initial DSM until the final DSM is satisfactory.

Surface Reconstruction for the Redwood Stand

The proposed model-based approach is built on top of conventional image matching algorithms. Both the conventional image matching and the model-based approach were implemented and applied to the redwood stand for a comparison. The 1-0 stereo pair was used as the primary pair for canopy surface reconstruction because more parts of the trees are visible in this pair. Other pairs were used for the areas occluded in the primary pair.

Conventional Surface Reconstruction

We first applied the dynamic programming algorithm to the conventional surface reconstruction without using tree models. Taking into consideration the large disparities caused by trees, the disparity range was estimated as $[-84, 38]$ (unit: pixels) for the primary stereo pair (1-0). For such a large disparity

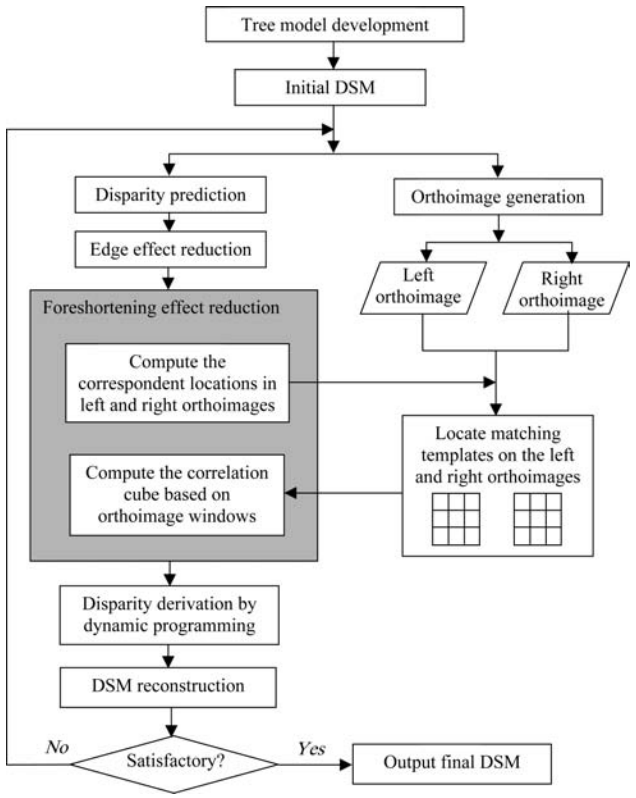

Figure 7. The sophisticated model-based canopy surface reconstruction scheme. This scheme incorporates occlusion removal, disparity prediction, edge-effect reduction, foreshortening effect mitigation, and iterative implementation.

range, the dynamic programming algorithm was implemented under the pyramidal matching scheme. For pyramidal matching efficiency, the disparity range was centralized to $[-61, 61]$ with a 23-pixel shift, and the right image was also shifted by the same amount of pixels. As a result, we used $[-61, 61]$ (i.e., $D = 61$) as the disparity range in the surface reconstruction, resulting in a four-level pyramid. The results of the pyramidal surface reconstruction using $p = 2$ are shown in Figure 8. The original left image (i.e., #1) is shown in Figure 8a as a reference. Figure 8b is the correlation strength map of the final level matching, showing that the ground (white areas) possesses good matching while the correlation measures over trees are low. Figure 8c shows the reconstructed surface model. The white margins in the surface model are noise induced by pyramidal resampling. The following can be observed from the surface model. The building on the right is clearly identifiable; the ground is reconstructed as a smooth surface; the stand surface is raised and rugged, but individual trees are not visible. Though having taken many constraints into consideration, the conventional matching scheme is sufficient for the ground surface, but it does not work well for the canopy surface. Therefore, it is necessary to introduce the model-based approach.

Model-Based Surface Reconstruction

We applied the proposed model-based scheme to reconstructing the canopy surface for the redwood stand. The initial values of D and p were set to $D = 3$, $p = 1$, and a smooth canopy surface was generated. The algorithm adjusts disparities around the predicted ones within a range of ± 3 pixels and has ± 1-pixel flexibility in controlling the smoothness of the disparity surface. With the configuration of the stereo pair 1-0, the disparity difference of 1 pixel corresponds to approximately a 0.4-m change in elevation in the ground coordinate system. Greater variation can be introduced to the surface by using larger D and p in the reconstruction. Larger D and p give the dynamic programming algorithm more freedom in disparity search, and thus allow greater variation in the reconstructed canopy surface. They may lead to more realistic results for the trees that are not well defined by their optimal tree model (e.g., Tree #32),

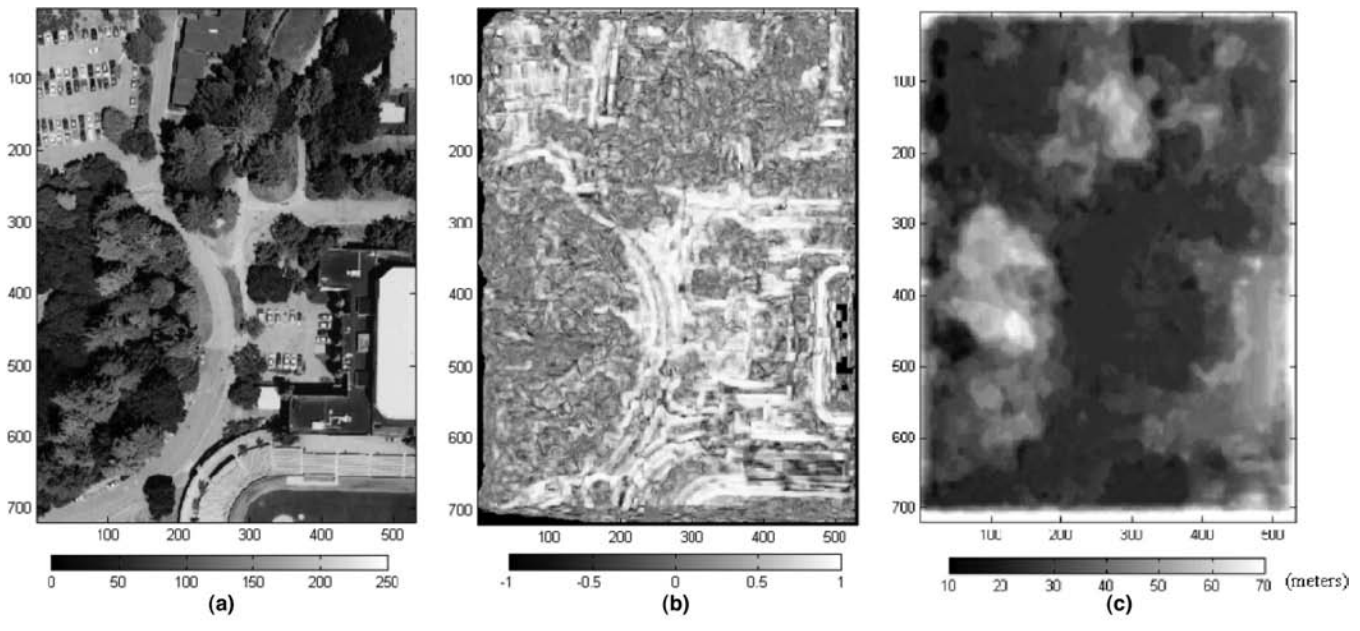

Figure 8. Results obtained with conventional image matching. (a) Left image. (b) Correlation map. (c) Reconstructed surface model.

TABLE 1. DISPARITY ADJUSTMENT UNDER DIFFERENT MATCHING CONTROLS

	Tree Properties			Iteration with $D = 3$, $p = 1$		
Tree-ID	Species	Tree shape	Tree model	Iteration 1	Iteration 2	Non-Iteration D = 6, p = 2
1	Redwood	Regular	Adequate	1.69*	1.01	2.96
32	Pine	Irregular	Inadequate	2.34	1.44	3.83

*Unit: pixels

but may corrupt the surface of the trees with an adequate tree model (e.g., Tree #1).

To achieve better results, the process was iterated twice using relatively small D and p (i.e., $D = 3$ and $p = 1$). Table 1 compares the degree of adjustment of the iterative and non-iterative implementation. The iterative reconstruction with smaller D and p regresses to the true surface gradually, while the non-iterative one with larger D and p makes a larger adjustment for all trees at one time. The surface derived for irregular-shaped trees (e.g., Tree #32) is adjusted more than that for regular-shaped ones (e.g., Tree #1). For trees with an adequate tree model, a major adjustment is made in the first round iteration, followed by a minor adjustment (about 1 pixel) in the second round. The iterative results are shown in Figure 9. Figures 9a and 9b show the final disparity map and the correlation strength map. Compared to the surface recovered from the conventional photogrammetric approach (Figure 8c), the one obtained from the model-based approach (Figure 9c) clearly shows individual trees. We used the iteratively reconstructed surface in the subsequent validation analysis.

Field Validation

Because it is difficult to directly measure canopy surface on the ground, we have to use alternatives to validate the reconstructed surface. Measurements of dimensional crown parameters such as tree height and crown radius, and crown profile pictures were collected on the ground. These dimensional parameters are used to check the size of reconstructed crowns, while the crown profile pictures are used to validate the reconstructed surface with detailed crown structures.

Crown radius and tree height were interactively extracted for individual trees from the reconstructed surface model in Figure 9c. In an interactive computer program, we place a circle on the surface model to surround a tree (i.e., a round object higher than its background in the surface model), and move the circle and resize it to make it fit the perimeter of the tree canopy. The DSM cells around the circle are crucial in determining the fitness. The inner circle edge consists of the DSM cells touching the circle from the inner side, and corresponds to the crown margin. Similarly, the outer circle edge contains the DSM cells touching the circle from the outside. When the contrast reaches the maximum between the averaged height ($\mathbf{H_0}$) of the outer circle edge and that of the inner edge, the circle is considered as the boundary between the tree and the background. The radius of the circle is considered as the crown radius, and the tree height is calculated as the difference between the maximum height of the cells within the circle and $\mathbf{H_0}$.

The tree parameters extracted from the reconstructed surface model and the ground measurements are listed in Table 2 for a comparison. We calculated the difference ΔH (or ΔR) between the DSM-derived parameters and ground measurements, and the ratio $\Delta H\%$ (or $\Delta R\%$) of ΔH (or ΔR) to the ground meas-

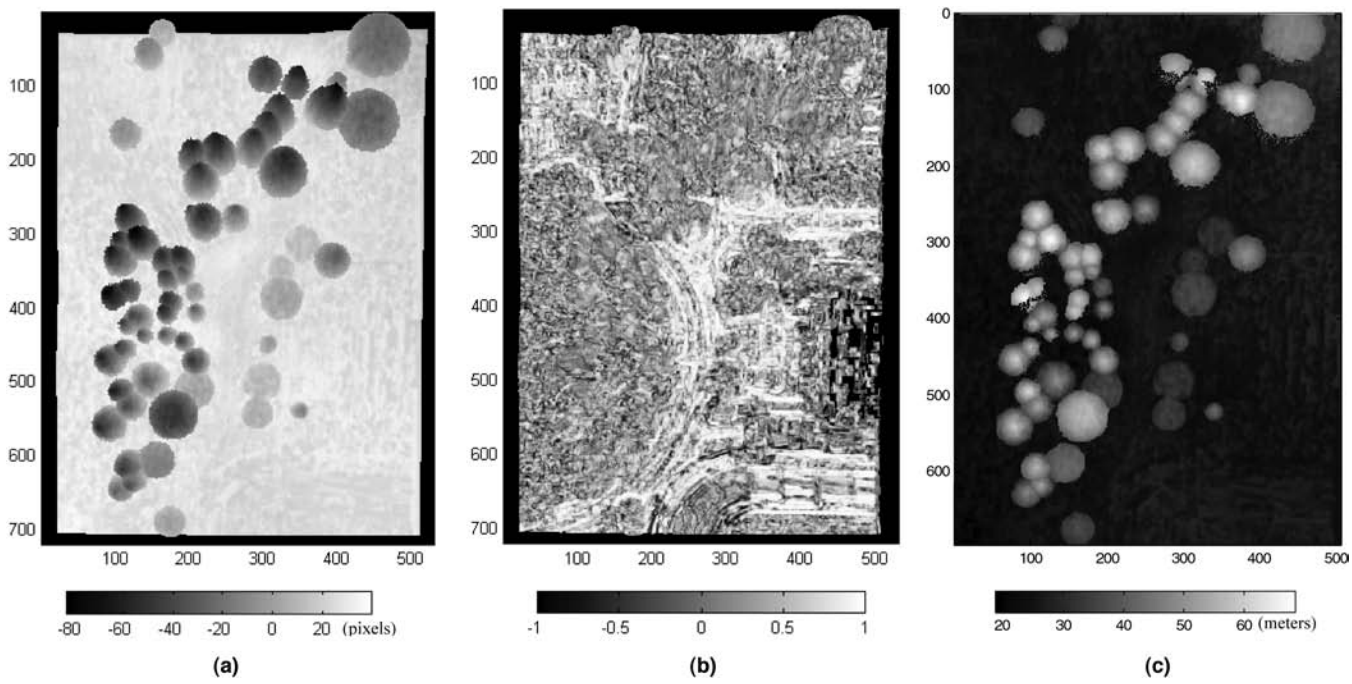

Figure 9. Results obtained with the iterative model-based canopy surface reconstruction. (a) Disparity map. (b) Correlation map. (c) Reconstructed surface model.

TABLE 2. GROUND VALIDATION FOR THE DIMENSIONAL CROWN PARAMETERS

		Field Measurements		DSM-Derived		Comparison			
Tree-ID	Species	Height(m)	R* (m)	Height (m)	R (m)	ΔH[+] (m)	ΔH%[X]	ΔR (m)	ΔR%
1	Redwood	27.7	4.9	25.2	4.9	−2.6	−9.2	0.0	0.4
2	Redwood	28.0	7.1	36.2	7.8	8.2	29.1	0.7	9.7
3	Redwood	33.2	6.7	28.3	5.7	−5.0	−14.9	−1.0	−15.0
4	Redwood	33.2	5.0	30.1	5.2	−3.2	−9.5	0.3	5.5
5	Redwood	36.3	5.8	33.6	6.1	−2.7	−7.5	0.3	5.8
6	Redwood	36.3	5.5	36.6	5.0	0.3	0.9	−0.4	−7.9
7	Redwood	34.7	6.6	34.1	6.0	−0.7	−1.9	−0.6	−8.7
8	Redwood	31.1	5.6	31.5	5.4	0.4	1.4	−0.1	−2.3
9	Redwood	31.1	3.1	30.3	2.7	−0.8	−2.7	−0.4	−14.0
10	Redwood	18.3	3.4	16.9	3.6	−1.3	−7.4	0.2	6.3
11	Redwood	25.9	2.8	25.2	3.3	−0.7	−2.8	0.5	16.2
12	Redwood	33.8	2.5	30.5	3.6	−3.3	−9.7	1.0	41.0
13	Redwood	32.3	2.7	34.0	2.7	1.7	5.4	0.0	0.0
14	Redwood	31.1	2.7	27.7	2.9	−3.4	−10.8	0.2	8.3
15	Redwood	35.4	4.2	35.3	4.3	−0.1	−0.2	0.1	2.8
16	Redwood	33.8	4.5	30.4	4.6	−3.4	−10.1	0.1	2.9
17	Redwood	33.2	3.9	27.7	3.8	−5.6	−16.7	−0.1	−1.4
18	Redwood	38.4	4.8	39.0	4.6	0.6	1.5	−0.2	−4.7
19	Redwood	34.4	4.7	34.0	4.8	−0.5	−1.3	0.1	2.7
20	Redwood	36.0	4.2	30.0	3.8	−5.9	−16.5	−0.4	−9.6
21	Redwood	39.9	5.5	37.8	5.3	−2.1	−5.2	−0.2	−3.6
22	Redwood	42.4	3.7	42.6	4.0	0.2	0.4	0.3	8.6
23	Redwood	32.0	3.6	37.7	3.2	5.7	17.7	−0.5	−13.1
24	Redwood	31.7	2.5	32.3	2.6	0.6	1.9	0.2	6.7
25	Redwood	29.9	4.3	29.7	4.7	−0.2	−0.6	0.4	10.2
26	Redwood	30.5	2.4	29.3	2.5	−1.2	−4.0	0.2	6.4
27	Redwood	32.3	3.2	32.3	3.4	0.0	0.1	0.2	7.8
28	Redwood	36.6	4.8	35.8	5.0	−0.7	−2.0	0.2	4.5
29	Redwood	28.3	3.0	28.7	3.2	0.4	1.3	0.2	8.3
30	Redwood	29.3	2.9	27.8	3.1	−1.5	−5.1	0.3	9.1
31	Redwood	27.7	4.1	27.7	4.5	−0.1	−0.2	0.5	11.1
32	Pine	30.5	6.8	31.7	8.2	1.2	4.0	1.4	20.1
33	Redwood	18.9	5.7	18.5	6.0	−0.4	−2.3	0.3	5.0
34	Redwood	29.3	4.7	28.7	4.6	−0.6	−2.0	−0.1	−1.3
35	Redwood	26.5	4.3	25.3	4.3	−1.2	−4.6	0.0	0.7
36	Redwood	21.3	4.3	21.1	4.3	−0.2	−0.9	0.0	0.9
37	Oak	11.0	5.5	11.5	5.3	0.5	4.8	−0.1	−2.3
38	Oak	7.3	5.7	9.4	5.2	2.1	28.3	−0.4	−7.7
Average						−0.67	−1.4	0.08	2.9
Mean absolute error[$]						1.8	6.4	0.3	7.7
Overall accuracy[#]							93.6		92.3

*R is the average of the four perpendicular crown radius readings in the field.
[+]ΔH is the difference between the DSM-derived tree height and the height measured in the field. ΔR is the difference of crown radius between photo measured and field measured.
[X]ΔH% is the ratio (in percentage) of ΔH to the tree height measured in the field. ΔR% is similarly defined for crown radius.
[$]The mean absolute error of ΔH (or ΔH%, ΔR and ΔR%) is defined as the average of the absolute values of ΔH (or ΔH%, ΔR and ΔR%) for all trees.
[#]The overall accuracy of tree height (or crown radius) is defined as 100 − mean absolute ΔH% (or ΔR%).

urement in percentage. The mean absolute error of tree height (or crown radius) is defined as the average of the absolute values of ΔH (or ΔR) for all trees. The overall accuracy of tree height (or crown radius) is defined as 100 − mean absolute ΔH% (or ΔR%).

We compared the derived crown radius with the average of the four ground radius readings. The overall accuracy is estimated as 92.3 percent, and the mean absolute error is 0.3 m. The derived crown radius of 87 percent trees is within an error of 0.5 m. For tree height, the mean absolute error is 1.8 m, and the overall accuracy is estimated as 93.6 percent. Seventy-six percent trees have an error of less than 3 m in tree height, and 79 percent trees have their height estimated with an accuracy of better than 90 percent. The worst case is Tree #2, the height of which is overestimated by 8.2 m. The discrepancy is caused by the inadequacy of the tree model. It was difficult to locate the treetop of Tree #2 on the photos during its model establishment. The DSM-derived parameter underestimates tree height by 0.67 m on average, and more trees (25 out of 38) were underestimated than overestimated in height. This may be partially explained by the five-year time lag between the field measurements and the aerial photos, and the fact that the sharp tips of conifers may not be captured in the images. In general, the dimensional parameters derived from the reconstructed surface model are quite close to the field measurements.

To examine the quality of the surface reconstructed for tree crowns of different levels of shape regularity, three trees were selected for a detailed validation using their profile pictures: a regular-shaped redwood (Tree #1), an intermediately regular-shaped oak tree (Tree #37), and an irregular-shaped pine tree (Tree #32).

The redwood tree is in a regular conic shape (with four crown radius readings of 4.8 m, 5.0 m, 5.0 m, and 4.9 m) as shown in the ground picture taken from the west direction (Figure 10a). The north-south profiles of the reconstructed crown surface shown in Figure 10b are consistent with the ground observations. The extended branches marked by **A** in the picture from the west view (Figure 10a) are also visible in the profiles (marker **A** in Figure 10b).

The four radius readings for the oak tree are 4.0 m, 4.4 m,

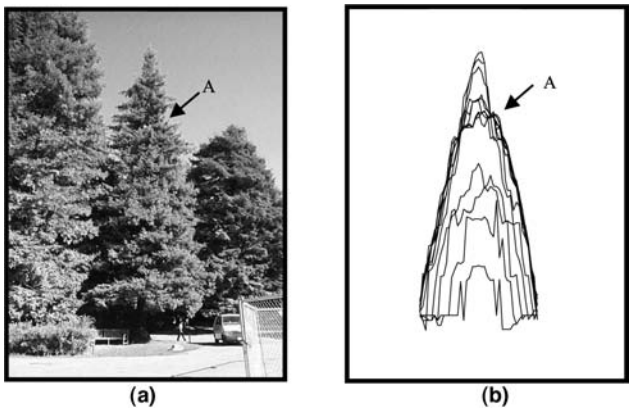

Figure 10. Ground truthing of Tree #1. (a) West view photo. (b) North-south profiles. This is the case of a regular-shaped redwood tree.

5.6 m, and 7.9 m. It was measured 11.0 m tall on the ground, and the reconstructed height is 11.5 m. Figures 11a and 11c show the ground pictures of the tree taken from the west and northeast directions, respectively. The corresponding profiles created from the reconstructed surface (Figures 11b and 11d) generally match the outlines shown in the ground pictures, and the surface features (marked by **A** and **B**) on the pictured profiles are also found in the reconstructed profiles.

The four ground crown radius readings of 11.2 m, 6.1 m, 2.0 m, and 8.0 m indicate that the pine tree is rather irregular in shape. Its ground picture and the reconstructed profiles are shown in Figure 12. Comparing the ground picture taken from the south (Figure 12a) with the corresponding profiles (Figure 12b) from the reconstructed surface, it is apparent that the general outline matches, but disagreements are also observable.

Discussions and Conclusions

From the experiments described in this paper, it has been demonstrated that canopy surface reconstruction can be considerably improved after tree models are introduced into the conventional image matching algorithm. However, a number of limitations remain:

- Limitations of the symmetric tree model: Though the symmetric tree model used in this paper can describe most conifers well, it may not adequately describe irregular ones. The symmetric tree model used in this paper needs to be upgraded for irregular-shaped trees.
- Surface sensitivity to tree models: Because the model-based matching algorithm is guided by tree models, the reconstructed surface is sensitive to these tree models. Adequate tree models are critical to the success of high-quality canopy surface reconstruction. If a model approximates the true surface with an offset

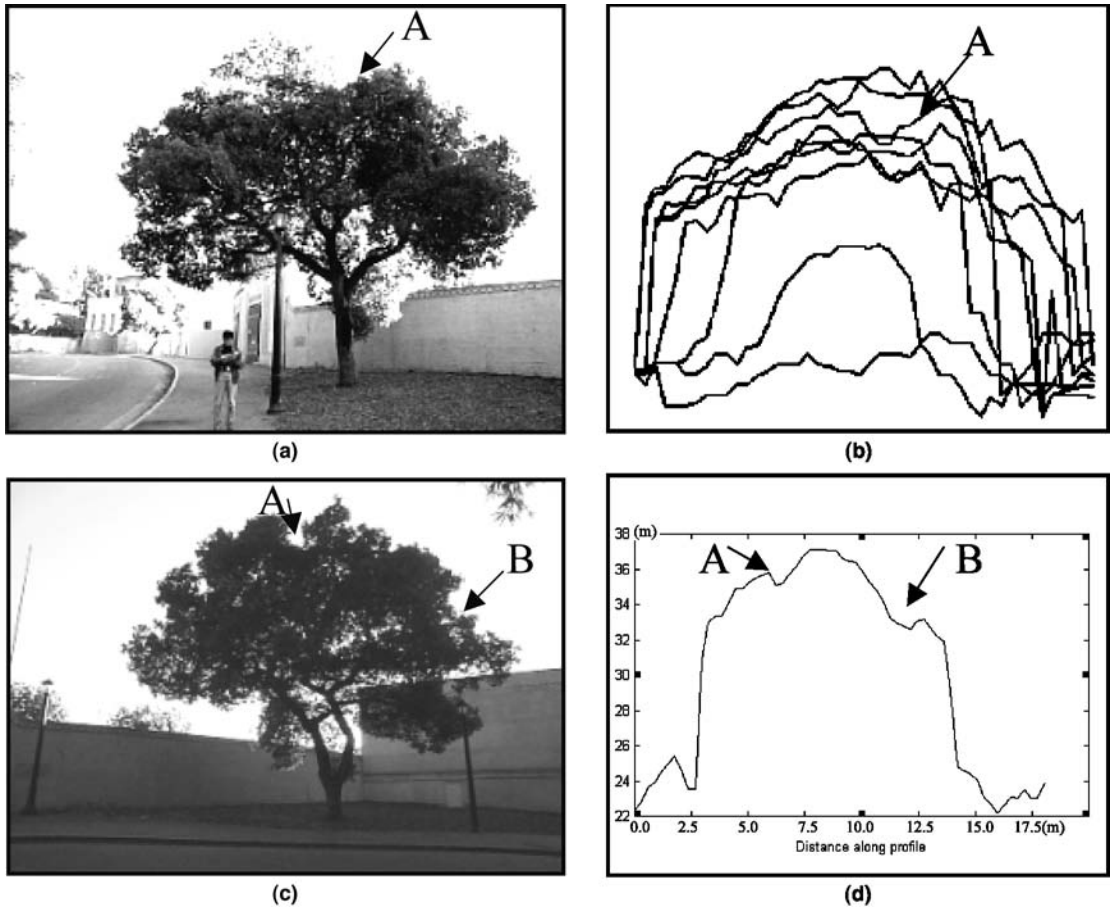

Figure 11. Ground truthing of Tree #37. (a) West view photo. (b) North-south profiles. (c) Northeast view photo. (d) Southeast-northwest profile. This is the case of an intermediately regular-shaped oak tree.

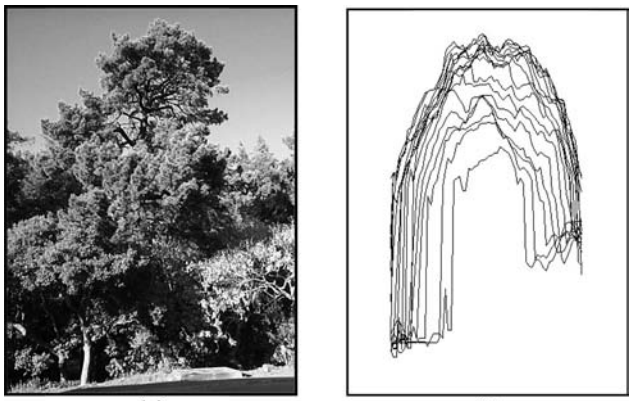

Figure 12. Ground truthing of Tree #32. (a) South view photo. (b) West-East profiles. This is the case of an irregular-shaped pine tree.

less than D pixels (D is the disparity limit) in the vertical dimension, it is possible to recover a qualified surface because the offset could be corrected by image matching. Otherwise, it is impossible to reconstruct a qualified surface from the model-based approach.

- Automation in tree model development: Tree models were developed semiautomatically using the 3D tree interpreter. Automation of this process is desirable, and it may be possible for less complicated stands. Because tree models are critical to successful canopy surface reconstruction, the quality of tree models automatically developed should be carefully examined.
- Factors affecting the accuracy of the reconstructed surface: Because reliable crown surface data are difficult to collect in the field, a quantitative analysis of factor influence on canopy surface reconstruction was not undertaken. The following factors may affect the accuracy: tree models, surface order p, the accuracy of photo-orientation parameters, image quality, stand complexity, and strong winds when aerial photographs were taken.

In conclusion, this paper starts with a conventional stereo-matching algorithm, and develops a model-base approach to canopy surface reconstruction incorporating tree models to guide stereo matching. Although the conventional image-matching algorithm already takes into consideration many factors and constraints, it still fails to adequately reconstruct canopy surfaces. This is because the photogrammetric algorithm is designed to map terrain surfaces whereas conifer canopy surfaces are highly variable. Model-based canopy surface reconstruction dramatically improves the results because tree models are integrated to guide image matching for local adjustments of disparities. The introduction of tree models, to a large degree, enables the image-matching algorithm to match the right portion of the correct tree crown in the adjustment range. The degree of adjustment can be controlled by the disparity limit D and the surface order p in dynamic programming. When a tree is irregular in shape or its optimal tree model is inadequate, larger D and p may help to reconstruct a realistic surface by introducing more freedom to image matching. In addition, the iterative implementation of the model-based image-matching algorithm also improves canopy surface reconstruction.

This paper successfully extends the model-based scheme from the single tree level to the forest-stand level, and demonstrates the effectiveness of such an approach in canopy surface reconstruction. To reconstruct canopy surfaces for the dense redwood stand, the following critical problems were addressed in the model-based canopy surface reconstruction process:

- occlusion in disparity prediction from tree models,
- integration of the predicted disparities into image matching,
- the tree-edge effect on the disparity map, and
- the foreshortening effect in image matching, which is very serious for conifer crown surfaces.

Solutions to the above problems are necessary for successful canopy surface reconstruction.

References

Biging, G.S., and S.J. Gill, 1997. Stochastic models for conifer tree crown profiles, *Forest Science*, 43(1):25–34.

Chen, Q., and G. Medioni, 1999. A volumetric stereo matching method: Application to image-based modeling, *Proceedings of the 1999 IEEE Computer Society Conference on Computer Vision and Pattern Recognition*, 23–25 June, Fort Collins, Colorado, 1:29–34.

Gong, P., Y. Sheng, and G.S. Biging, 2002. 3D model-based tree measurement from high resolution aerial imagery, *Photogrammetric Engineering & Remote Sensing*, 68(11):1203–1212.

Horn, H.S., 1971. *The Adaptive Geometry of Trees*, Princeton University Press, Princeton, New Jersey, 144 p.

Klaus, B., and P. Horn, 1986. Photogrammetry & stereo, *Robot Vision* (B. Klaus and P. Horn, editors), The MIT Press, Cambridge, Massachusetts, pp. 299–333.

Marr, D., 1982. *Vision: A Computational Investigation into the Human Representation and Processing of Visual Information*, W. H. Freeman and Company, New York, 397 p.

Norvelle, F.R., 1992. Stereo correlation: Window shaping and DEM corrections, *Photogrammetric Engineering & Remote Sensing*, 58(1):111–115.

———, 1996. Using iterative orthophoto refinements to generate and correct digital elevation models (DEM's), *Digital Photogrammetry: An Addendum to the Manual of Photogrammetry* (C. Greve, editor), American Society for Photogrammetry and Remote Sensing, Bethesda, Maryland, pp. 151–155.

Pokorny, C.K., and C.F. Gerald, 1989. *Computer Graphics: The Principles Behind the Art and Science*, Franklin, Beedle & Associates, Irvine, California, 738 p.

Pollock, R.J., 1996. *The Automatic Recognition of Individual Trees in Aerial Images of Forests Based on a Synthetic Tree Crown Image Model*, Ph.D. dissertation, University of British Columbia, Vancouver, Canada, 172 p.

Quackenbush, L.J., P.F. Hopkins, and G.J. Kinn, 1999. Developing derivative products from high resolution digital aerial imagery, *Proceedings of the ASPRS 1999 Annual Convention*, 19–21 May, Portland, Oregon (American Society for Photogrammetry and Remote Sensing, Bethesda, Maryland), unpaginated CD-ROM.

Schenk, T., and C.K. Toth, 1992. Conceptual issues of softcopy photogrammetric workstations, *Photogrammetric Engineering & Remote Sensing*, 58(1):101–110.

Sheng, Y., 2000. *Model-Based Conifer Crown Surface Reconstruction from Multi-Ocular High-Resolution Aerial Imagery*, Ph.D. dissertation, University of California at Berkeley, Berkeley, California, 168 p.

Sheng, Y., P. Gong, and G.S. Biging, 2001. Model-based conifer crown surface reconstruction from high-resolution aerial images, *Photogrammetric Engineering & Remote Sensing*, 67(8):957–965.

Sun, C., 1999. Multi-resolution stereo matching using maximum-surface techniques, *Proceedings of Digital Image Computing: Techniques and Applications*, 07–08 December, Perth, Australia, pp.195–200.

———, 2002. Fast stereo matching using rectangular subregioning and maximum-surface techniques, *International Journal of Computer Vision*, 47(1/2/3):99–117.

(Received 09 February 2001; revised and accepted 23 September 2002)